Viscoelasticity of the sarcomere matrix of skeletal muscles

The titin–myosin composite filament is a dual-stage molecular spring

Kuan Wang,* Roger McCarter,‡ John Wright,* Jennate Beverly,‡ and Ruben Ramirez-Mitchell*

*Clayton Foundation Biochemical Institute, Department of Chemistry and Biochemistry, Cell Research Institute, University of Texas at Austin, Austin, Texas 78712; and the ‡Department of Physiology, University of Texas Health Science Center at San Antonio, Texas 78284 USA

ABSTRACT The mechanical roles of sarcomere-associated cytoskeletal lattices were investigated by studying the resting tension–sarcomere length curves of mechanically skinned rabbit psoas muscle fibers over a wide range of sarcomere strain. Correlative immunoelectron microscopy of the elastic titin filaments of the endosarcomeric lattice revealed biphasic extensibility behaviors and provided a structural interpretation of the multiphasic tension-length curves. We propose that the reversible change of contour length of the extensible segment of titin between the Z line and the end of thick filaments underlies the exponential rise of resting tension. At and beyond an elastic limit near 3.8 μm, a portion of the anchored titin segment that adheres to thick filaments is released from the distal ends of thick filament. This increase in extensible length of titin results in a net length increase in the unstrained extensible segment, thereby lowering the stiffness of the fiber, lengthening the slack sarcomere length, and shifting the yield point in postyield sarcomeres. Thus, the titin–myosin composite filament behaves as a dual-stage molecular spring, consisting of an elastic connector segment for normal response and a longer latent segment that is recruited at and beyond the elastic limit of the sarcomere.

Exosarcomeric intermediate filaments contribute to resting tension only above 4.5 μm. We conclude that the interlinked endo- and exosarcomeric lattices are both viscoelastic force-bearing elements. These distinct cytoskeletal lattices appear to operate over two ranges of sarcomere strains and collectively enable myofibrils to respond viscoelastically over a broad range of sarcomere and fiber lengths.

INTRODUCTION

A quiescent skeletal muscle is remarkably elastic. It bears tension when it is stretched and then snaps back to its original length when released. As muscle is activated, it shortens and develops tension and then relengthens to its original length when activation ceases. Despite the tremendous advance in the understanding of the roles of actin and myosin in active contraction (1–3), comparatively little is understood regarding the structural basis of the long-range elasticity and the mechanisms with which forces are generated to cause recoil of stretched muscle when released or relengthening of contracted ones.

Earlier physiological studies of muscle elasticity generally have been modeled as elastic elements either in series or in parallel with a contractile unit without specifying their anatomical origin (e.g., reference 4). Recent studies clearly indicate that within the physiological range of muscle length changes, the myofibrillar structures are the major source of elasticity and that the sarcolemma and extracellular connective tissues contribute significantly only in highly extended skeletal muscles (5). Because neither actin nor myosin filaments display long-range elasticity, sarcomere-associated cytoskeletons must play a predominant role. Prime candidates are two biochemically distinct but structurally interconnected lattices (6, 7). One is an exosarcomeric network of intermediate filaments that envelop and interconnect the sarcomeres to the membrane-associated skeleton (costamere) and organelles. Because sarcomeres are linked both radially to parallel myofibrils and longitudinally to adjacent sarcomeres of the same myofibrils at the Z and M lines, this intermediate filament network is potentially force bearing in muscle cells (6, 8–10). The second candidate is a newly recognized endosarcomeric matrix consisting of both a set of extensible titin filaments that span between the Z line and the M line region and a set of inextensible nebulin filaments that act as templates for thin filaments (for reviews see 7, 11–14). In the intact sarcomere, a single titin polypeptide spans half a sarcomere and consists of two mechanical segments: the segment between the Z line and the edge of A band is extensible, whereas the segment within the A band is anchored and prevented from stretching presumably by its interaction with thick filaments or associated proteins (15–19). This titin–myosin composite filament thus displays segmental extensibility.

The structural features of these cytoskeletal lattices have been elucidated to such a degree that insightful correlative studies of muscle mechanics and structure can be designed. So far, several experimental approaches have been taken to evaluate the contribution of sarcomere lattices to muscle elasticity. One is to correlate the reduction of resting tension with the preferential destruction or removal of protein components, e.g., in studies where titin was destroyed by radiation (20) or by controlled proteolysis (21). A second approach is to model the behavior of thick filament translocation during iso-

Address correspondence to Dr. Kuan Wang, Department of Chemistry and Biochemistry, The University of Texas at Austin, Austin, Texas 78712, USA.

0006-3495/93/04/1161/17 $2.00

metric contraction on the presumptive elastic property of titin (22, 23). Both approaches have implicated titin in the resting tension and positional stability of thick filaments in the sarcomere. Despite these encouraging advances, the structural and molecular basis of muscle elasticity remain obscure. In this article, we address the following questions. (*a*) Are both the sarcomere matrix and the intermediate filament network force-bearing structures? If so, what are their relative contributions to resting tension? (*b*) How does the segmental extensibility of titin filaments manifest itself in the mechanical behavior of muscle sarcomeres? What are the roles of the extensible segment versus the anchored segment of titin? (*c*) How does the thick filament contribute to resting tension? To this end, we have measured resting tension as sarcomeres are stretched stepwise to well beyond their elastic limit and interpreted these multiphasic resting tension–sarcomere length curves by the relative contribution of viscoelasticity of the two types of sarcomere-associated lattices. Experimentally, this is accomplished by (*a*) direct measurement of extensibility of titin filaments (i.e., filament strain) by monitoring the translocation of titin epitopes with immunoelectron microscopy; (*b*) detecting ultrastructural changes of the titin–myosin composite filaments near the elastic limit (i.e., yield point) of the sarcomere; and (*c*) examining the mechanical responses of the exosarcomeric intermediate filament lattice subsequent to KI extraction.

Our analysis indicates that the entire stress–strain curve can be resolved into two sources of tensions that arise from, at low sarcomere strain, the reversible extension of a segment of titin that is free of the constraint imposed by thick filaments and, at higher sarcomere strain, from the reversible structural changes of the intermediate filament network at sarcomere length > 4.5 μm. Thus, both lattices are force-bearing structures but differ from each other both in the operative range of sarcomere strain and in their relative contribution to the total tension of the muscle fiber. We propose a novel concept that mechanically titin can be viewed as a dual-stage molecular spring that is highly extensible yet strong in tensile strength. We formulate a segmental extension model as a testable working hypothesis that is consistent with known structural and mechanical behaviors of the sarcomere and the general design principles of biological composite material.

EXPERIMENTAL PROCEDURES

Split muscle fiber preparation

On the day of each experiment, thin strips (3-mm wide) of fresh rabbit psoas muscle tissues (New Zealand white, 1.0–2.0 kg body weight) were removed within 10 min postmortem and immersed in a relaxing buffer containing protease inhibitors (150 mM K propionate, 5 mM KH_2PO_4, 3 mM Mg acetate, 5 mM ethyleneglycol-bis(β-aminoethyl ether)-*N,N'*-tetraacetic acid [EGTA], 5 mM Na azide, and 3 mM adenosine triphosphate [ATP]; 0.1 mM dithiothreitol [DTT], 5 μg/ml aprotinin, and 20 μg/ml leupeptin, pH 7.0) for 3 h at 4°C in a Sylgard dish. Single fibers were separated, pinned down at the ends with stainless steel pins, and then mechanically skinned by grasping a small bundle of surface myofibrils and pulling them gently away to roll up the sarcolemma (24). For mechanical and structural studies, the portion of denuded split fibers that remained affixed at both ends in the Sylgard was used, because it was not strained during skinning. All tension data reported in this article were obtained from fresh fibers used within 7 h postmortem.

Stress–strain curves of split fibers

The split fiber was placed in a glass chamber (2 ml) and mounted between a force transducer (model 400A; Cambridge Technology, Cambridge, MA) and a muscle ergometer (model 300S; Cambridge Technology) that was mounted on a motor-driven micromanipulator (MM3-33, Narashige Scientific Laboratory, Tokyo, Japan). A small piece of T-shaped platinum foil was squeezed with tweezers onto each end of the split fiber and attached via a hole in each foil to the transducer and the ergometer. Care was taken not to twist the fiber during mounting. Signals to and from the transducer and servo-motor were interfaced to an IBM PC by an Isaac 2000 A/D system (Cyborg, Cambridge, MA) and simultaneously recorded on an analog strip chart recorder. Solutions entered at the base and exited from the top of the chamber via a peristaltic pump at the rate of 20 ml/h to maintain a relaxing environment without an ATP-replenishing system. All experiments were conducted at room temperature (24°C).

Sarcomere length and fiber width were measured at three different locations along the preparation using a water immersion lens (40×; Zeiss, Thornwood, NY) and a filar micrometer. Sarcomere length was also monitored during the course of an experiment by measuring the first-order diffraction lines of a He-Ne laser beam (3 mW, 0.8-mm beam diameter, model 120; Spectra-Physics Inc., Mountain View, CA). For a given stretch-release cycle, the fiber, after the slack fiber length and sarcomere length were recorded, was slowly stretched stepwise in intervals of 10% of the slack fiber length over 30 s by a computer program that controlled the motor-driven micromanipulator. At the end of each stretch, fiber length was held constant for 150 s to allow tension to decay exponentially to within 85–90% of the value after 40–60 min of relaxation (our unpublished observations). After a given number of stretches to a desired fiber length, the fiber was then released stepwise in the same fashion, causing the tension to dip and then rise to a plateau value upon each release. The fiber frequently became slack before its complete return to the prestretch micrometer setting. However, the fiber eventually picked up the slack within 5–10 min, and its sarcomere length returned to either prestretch values for those fibers that were subjected to preyield stretch (below 3.8 μm) or to a slightly higher length for fibers subjected to postyield stretch (above 4.0 μm). Due to this length creep phenomenon, additional cycles of stretch–release, when performed, were followed by a 20-min rest period between cycles. In all experiments, plots of fiber length versus sarcomere length were monitored to detect slippage of fibers at points of attachment. Only those fibers that displayed linear plots with slope = 1 were considered further.

Stress–strain curves of exosarcomeric intermediate filament network

The sarcomere-associated intermediate filament networks were prepared by first subjecting split muscle fibers to one cycle of stretch–release (up to 6 μm and then returned) in the relaxing buffer while monitoring tension, followed by irrigating with 0.6 M KI, 0.1 M tris(hydroxymethyl)-aminomethane·Cl, 3 mM EGTA, 3 mM $MgCl_2$, 3 mM $Na_2P_2O_7$, 5 mM $Na_2S_2O_3$, 0.1 mM DTT, pH 7.5, for 10 min at 22°C. The residual structure was washed twice with the KI buffer to remove solubilized proteins and then twice with the relaxing buffer before further mechanical measurements. The conditioning of fibers by this

preextraction cycling somehow rendered the sarcomere striations more resistant to KI extraction and allowed sarcomere length to be measured reliably by light microscopy and by laser diffraction. Extraction of unconditioned fibers frequently resulted in distorted and smeary striation that were difficult to measure and, as a result, only fiber length was obtainable.

Electron microscopy

To facilitate structural and mechanical correlation, several split fibers were fixed in the chamber after tension measurement and processed for electron microscopy. This was accomplished by replacing relaxing buffer with 2% glutaraldehyde in 0.05 M sodium cacodylate, pH 7.2, for 60 min at 0°C. Fibers fixed in this manner resisted further stretch (causing a steep rise in tension) and did not shorten when severed and released from the platinum clips. The samples were held between gold oyster grids, osmicated by 1% OsO_4 in 0.05 M sodium cacodylate, pH 7.2, en bloc stained in uranyl acetate, dehydrated with ethanol, and embedded in Epon-Araldite (Ciba-Geigy, Hawthorne, NY). Thin sections were cut either longitudinally with the knife edge parallel to the fiber or cross-sectionally. Sections were stained with uranyl acetate and Reynolds lead citrate and observed with an electron microscope (model 100CX; JEOL USA, Inc., Peabody, MA) at 50–100 KV.

Immunoelectron microscopy

To quantitate the extension of titin segments, the stretch dependence of titin epitopes was investigated by immunoelectron microscopy with mouse monoclonal RT13 (to an I-band epitope) and RT15 (to an A-band epitope) essentially as described for nebulin labeling (24). Briefly, split fibers in the relaxing solution were hand-stretched to various degrees and attached to gold single slot grids, fixed in 3.7% formaldehyde, labeled with anti-titins or nonimmune mouse immunoglobulin as controls, followed by rabbit anti-mouse immunoglobulin and then protein A-gold bead conjugates, embedded in plastic, and sectioned. Epitopes were identified by stripes of antibody densities and, in postyield sarcomeres where significant broadening of labeling zone rendered it too diffuse to be detected by antibody density, by the distribution of the overlying gold beads in the electron micrographs. Epitope translocation was determined by plotting the center to center distance from epitope to the Z line or to the M line as a function of sarcomere length. The broadening of epitope zones was measured by plotting the width of antibody zones as a function of sarcomere length.

In some samples, split fibers were extracted with 0.6 M KCl, 2 mM EDTA, 2 mM $Na_2P_2O_7$, 0.1 mM DTT, pH 6.8, for 30 min at 0°C to extract A-band, washed twice, and followed by fixation, antibody labeling, and plastic embedding as described above. Epitopes in A-band–extracted sarcomeres were identified by gold bead clusters.

Thick filament counting

To estimate force-bearing capacity of individual titin filaments, especially at yield points (see below), the fiber was first stretched beyond yield point to record yield tension and then released and fixed at a fiber length close to or slightly above its slack length. Filament counting was facilitated near slack length since both fiber diameter and interfilament spacings were larger near slack length. A set of low magnification micrographs of fiber cross-sections as well as high magnification micrographs of A-bands of the same field were taken. Thick filament density per unit area of A-band and a total cross-sectional area of A- and I-bands were measured. Thick filament counts per split fiber were estimated by multiplying these two parameters. An assumption is made that the cross-sectional area of I-bands are equal to those of the A-bands that are adjacent but out of the section plane.

Data processing

Tension data for individual split fibers were plotted as a function of sarcomere length either as absolute values or as relative tensions normalized to the yield point individual tension of each fiber, depending on the degree of stretch. The use of yield point tension as the reference point is justified, since the yield point sarcomere length (SL_y) can be determined within 0.1–0.2 μm and exhibited very little variation among individual fibers for a given muscle tissue and rate of stretch (our unpublished observations). Furthermore, the yield point normalized tension is expected to be proportional to the cross-sectional area and total number of titin–myosin composite filaments across the fibers.

For statistical analysis (Statographics version 4.0; Manugistics, Rockville, MD), the data sets were grouped into classes based on sarcomere length (0.2-μm intervals). Moving average analysis was done by averaging over one point on each side of the target value. The endpoints were calculated by linear extrapolation, and the fitted lines were drawn between the points. Nonlinear regression analysis of the exponential region was done on a subset of the stretch curve corresponding to the linear portion of log tension versus sarcomere length plot.

A similar set of statistical parameters were calculated after recording the data for epitope translocation data (Ab-Z distance) and epitope width (Ab-zone). The averages for each class were used for further analysis.

Image analysis and average thick filament length

Electron micrographs of normal and stretched sarcomeres were digitized with a Megavision 1000 line scanner and processed with a Megavision 1024 XM image processing system (Megavision, Goleta, CA). Images were acquired by accumulating 50 consecutive images. A regular polygon with a height equal to the fibril diameter and a length extending beyond the width of the A-band was used as a mask and divided into 64 regions with a wedge consisting of 64 vertical gray-level wedges. This image was binarized by thresholding until the vertical regions consisted of white bands (14 pixels wide) separated by black vertical bands (2 pixels wide). Density, mass, and x-centroid for the 64 regions were then measured. The gray-level density was plotted against the x-centroid to give the density profile. The average thick filament length is defined as the full width at half-maximum of the density-profile of the A-band.

The yield point was calculated as the first local maximum in each tension–length curve. The exponential curve was normalized to this value, and data sets for all muscle fibers were merged.

RESULTS

Viscoelasticity of split muscle fibers

The split fiber preparation is uniquely suited for detailed correlative studies of sarcomere structure and mechanical behaviors because (*a*) it is free of the sarcolemma and extracellular matrix that would contribute to the resting tension of intact or chemically skinned muscle fibers in yet unspecified manners; (*b*) it can be stretched to nearly three times its resting length without breakage or excessive loss of striation, thus facilitating correlation over a wide range of sarcomere length; (*c*) it is amenable to immunoelectron microscopy and ultrastructural analysis, thus permitting correlative structural studies; and (*d*) it is easily prepared from a wide range of muscle fibers irrespective of the amount of connective tissues, thus facilitating comparative studies of different tissues.

When split fibers were stretched or released in small increments, their mechanical responses were viscoelastic and were similar to those reported for whole muscle tissues and intact or skinned single muscle fibers (e.g., 5, 25, 26). Upon each stretch, tension quickly rose to a

peak and then decayed exponentially toward a steady-state plateau value. Similarly, upon each release, the tension dropped and then rose slightly toward a new plateau level (Fig. 1). This stress–relaxation took place without a detectable change in sarcomere length, and the relaxation process could be resolved into two or three single exponential decays with different rate constants, varying with both the sarcomere length and the magnitude and speed of length change (our unpublished observations). We have operationally defined the plateau tension as the value after 150 s of relaxation which, for experiments reported here, is within 85–90% of the tension after 40–60 min of relaxation. These fibers also display significant hysterisis as evidenced by the observation that tensions developed during stretch, either the peak or the plateau tension, always exceed those developed during release at the same sarcomere length (Fig. 1). Both stress–relaxation and hysteresis are commonly observed phenomena with viscoelastic biological tissues and reflect the fact that the structure requires time to respond and that the magnitude of mechanical response varies with both the extent and the direction of strain (i.e., stretch versus release).

Because our primary objective here is to correlate mechanical properties with structural features of titin filaments in the sarcomere that can be monitored by immunoelectron microscopy, we chose to focus on the study of the steady-state plateau tension measured after stress–relaxation, rather than the analysis of the dynamic stress–relaxation that changes rapidly with time. Experimentally, the resting tension–length curve of a split fiber was measured by stepwise stretch or release while monitoring its sarcomere length by laser diffraction. The unit slope of the linear plot of fiber length versus sarcomere length was used as a quality control to detect deviation resulting from slippage at the platinum clips (Fig. 1, *inset*). For direct structural correlation, a few fibers were fixed at various points along the tension–length curve and processed for electron microscopy. In parallel experiments, the elastic behavior of titin filaments were investigated in a large number of split fibers by quantitating the stretch dependence of titin epitopes with immunoelectron microscopy (see Fig. 3).

Multiphasic resting tension–sarcomere length curves of split fibers

A representative plot of plateau tension versus sarcomere length of rabbit psoas split fibers that were stretched from slack length to ~5.5 μm displayed a characteristic multiphasic curve (Fig. 2 *A*): as the fiber was stretched stepwise beyond slack sarcomere length (SL_0) around 2.2 μm, little or no tension was detected until 2.5–2.6 μm (SL_e, see Discussion and Fig. 8). Beyond this point, tensions increased exponentially and then peaked and leveled around 3.8–3.9 μm (designated as SL_y). Further stretching beyond 4.5 μm caused the tension to rise further until the fiber began to lose striation and be torn apart. The tension–length curve in the release direction was qualitatively different from the stretch curve in that the tension decreased steeply with reduction in sarcomere length (Figs. 2 *A* and 6). In the example shown in Fig. 2, the highly stretched fiber that was released from 4.5 μm became slack around 3.0 μm. However, when the fiber was allowed to rest for 5–20 min at a micrometer setting corresponding to the slack

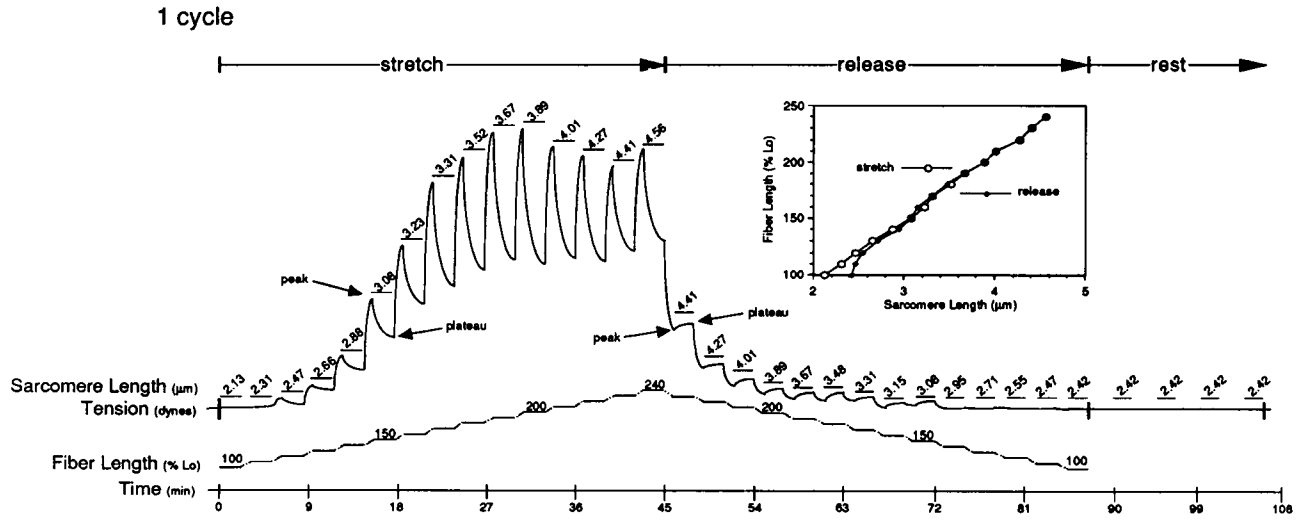

FIGURE 1 Mechanics protocol. Tension, sarcomere length, and fiber length were recorded as a rabbit psoas split fiber in relaxing solution was subjected to a cycle of stepwise stretches and releases (10% per step per 30 s) followed by a rest phase (20 min). Tension rose during stretch to a "peak" value and relaxed toward a "plateau" value when the fiber was held constant for 150 s. Similarly, tension dropped and recovered toward a plateau value after each release. The unit slope of the linear plot of sarcomere length versus fiber length (*inset*) was used as a criterion of a firm clip-hook attachment. Note that after a postyield point stretch to 4.56 μm, the totally released fiber had a longer slack sarcomere length at 2.42 μm (from a prestretch value of 2.3) that remained constant for ≥20 min.

fiber length before stretch, its sarcomere length gradually crept from 3.0 μm back to a new slack length at 2.4 μm. In contrast, if the stretch did not exceed the yield point, the fiber would, after a similar rest period, return completely to the original slack sarcomere length of 2.2 μm (see Fig. 6). For this reason, a rest period of 20 min was routinely applied before the next cycle of stretch–release. It is significant that plots of either peak or plateau tension are qualitatively similar, displaying the same SL_0 and SL_y and significant amount of hysteresis (not shown; see reference 27).

Viscoelasticity of the intermediate filament network: resting tension–sarcomere length curves of KI-extracted split fibers

To evaluate the mechanical contribution of intermediate filaments, the split fiber was first subjected to one cycle of stretch–release to 5.5–6.0 μm, released to slack length, and then extracted with a 0.6 M KI buffer. The KI treatment, as we have shown previously (10), disassembled thick and thin filaments, dislodged titin filaments at the end near the M line and caused titin (and nebulin) to translocate and accumulate near the Z line anchor. As a result, the only mechanically competent lattice in the residue is the sarcomere-associated intermediate filaments that have resisted the disruptive effect of KI. The conditioning of fibers by cycling close to 6.0 μm somehow rendered the sarcomere striation more resistant to KI extraction and allowed the sarcomere length to be measured after extraction. As shown in Fig. 2 *B*, the KI residue was very compliant, and tension was detected only beyond 4.5 μm and rose at longer lengths to as much as 5 dynes at 5.2 μm for this fiber. A small hysteresis was observed during release (Fig. 2 *B*). Although the absolute magnitude and the slope of tension rise of KI residue varied among 10 different fiber preparations, it is significant that each KI curve was consistently similar in magnitude to the rise in tension beyond 4.5 μm of the same fiber before extraction. This resemblance suggests that the extension of the intermediate filament network is responsible for the increase in tension beyond 4.5 μm. Thus, the exosarcomeric intermediate filament network is a viscoelastic force-bearing structure that is slack below 4.5 μm. Upon further stretch, it develops significant tension amounting to as much as one quarter of the yield point tension of the same fiber.

Viscoelasticity of the sarcomere matrix: a biphasic resting tension–sarcomere length curve during stretch

The contribution of the sarcomere matrix to resting tensions was calculated by subtracting the KI-residue curve from the preextraction curve of the same fiber. As expected, the resulting curve differs only in the region beyond 4.5 μm: tension initially rose exponentially,

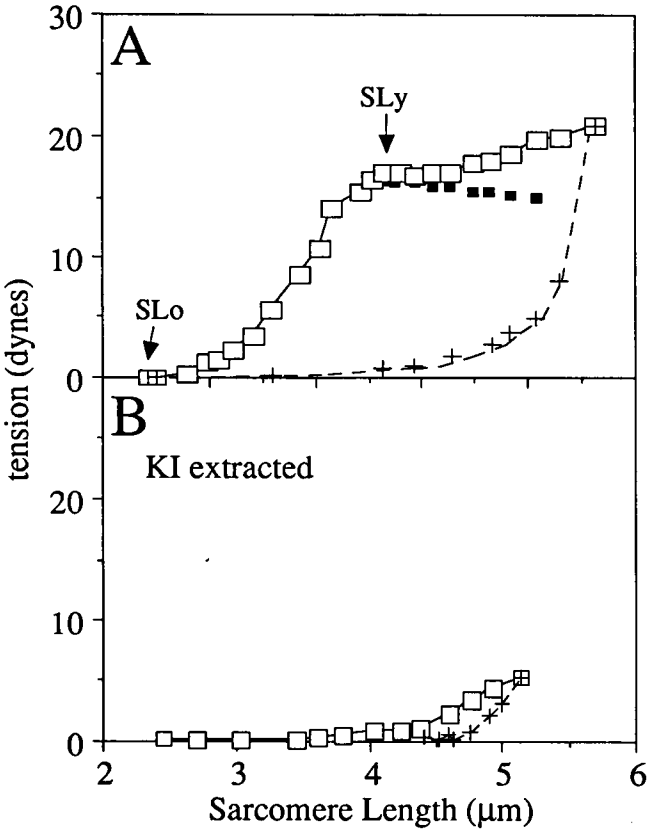

FIGURE 2 Resting tension–sarcomere length curve of a passive fiber before and after KI extraction. Plateau tension and sarcomere length of a split fiber in relaxing solution were determined 150 s after each stretch step (as in Fig. 1) until sarcomere length reached 5.5 μm (□). The fiber was released stepwise (+,+) to slack length and then treated with a KI buffer to extract both myosin and actin filaments before another stretch–release cycle. (*A*) Tension–length loop of unextracted fiber. During stretch, an exponential tension rise before the yield point (SL_y) is followed by a second tension rise after 4.5 μm. The release curve has much reduced tension at a given sarcomere length, giving rise to significant hysteresis in the loop. (*B*) Tension–length loop of KI residue. KI extraction abolished all tension up to 4.5 μm. The loop with a small hysteresis is similar in magnitude to the rise in tension beyond 4.5 μm in *A*. The difference in stretch curves before and after KI extraction, due to sarcomere matrix, was calculated and the values after SL_y were plotted in *A* (■).

reached a yield point and then leveled from 4.5 μm to ≥5.5 μm. These curves indicate that the sarcomere matrix is solely responsible for the first exponential tension rise before the yield point and contributes a nearly constant amount of tension at all degrees of extension of postyield point sarcomeres. The leveling of the curves suggest that the sarcomere matrix reached an elastic limit at the yield point and would thereafter elongate readily (another ~70%) with very little additional increase in tension.

Thus, the multiphasic tension–length curves of resting split fibers can be resolved into two components: one arises from the deformation of the endosarcomeric matrix starting as early as 2.6 μm; the second one results from the exosarcomeric intermediate filament network

appearing only at high sarcomere length (>4.5 μm) and eventually contributes as much as 20–30% of the total tension at 5.5 μm. The two distinct cytoskeletal lattices appear to operate over two ranges of sarcomere strains and collectively enable myofibrils to respond viscoelastically over a broad range of sarcomere and fiber lengths.

Segmental extensibility of titin filaments: biphasic epitope translation curves

The characteristic biphasic tension–length curve of the sarcomere matrix suggested that if titin is indeed directly involved in the development of resting tension, a major sarcomeric structural change involving titin should occur near the elastic limit (i.e., yield point). To search for such structural changes, we measured the extensibility of titin filaments throughout the entire range of sarcomere strain by studying the translocation of a pair of titin epitopes recognized by monoclonal anti-titin antibodies (RT13, RT15) with electron microscopy. As shown in Fig. 3, RT13 labeled a pair of titin epitopes in the I-band ~0.3 μm from the Z line in resting length sarcomeres (Fig. 3 *A*). The epitope staining broadened and moved away from the Z line in longer sarcomeres (Fig. 3 *B*). Further stretching to 3.7 μm caused the epitope zone to spread significantly and was discernible by the clusters of gold beads (Fig. 3 *C*). Over 4.2 μm, the gold clusters were scattered on the titin filaments that spanned the gap regions between the A-band and IZI segments (Fig. 3 *D*). In contrast, the epitopes recognized by RT15 were localized in the A-band at a constant distance (0.4 μm) away from the M line at all sarcomere lengths (Fig. 3, *A–D*). It is interesting that RT15 stained a pair of doublet in long sarcomeres (Fig. 3, *B–D*) yet only the one closest to the M line was observed in shorter sarcomeres (Fig. 3 *A*). Closer examination indicated that the outer member of the doublet's density was intrinsically weaker and was blocked or obscured by thin filaments in the overlapping zone of the shorter sarcomere (Fig. 3 *A*).

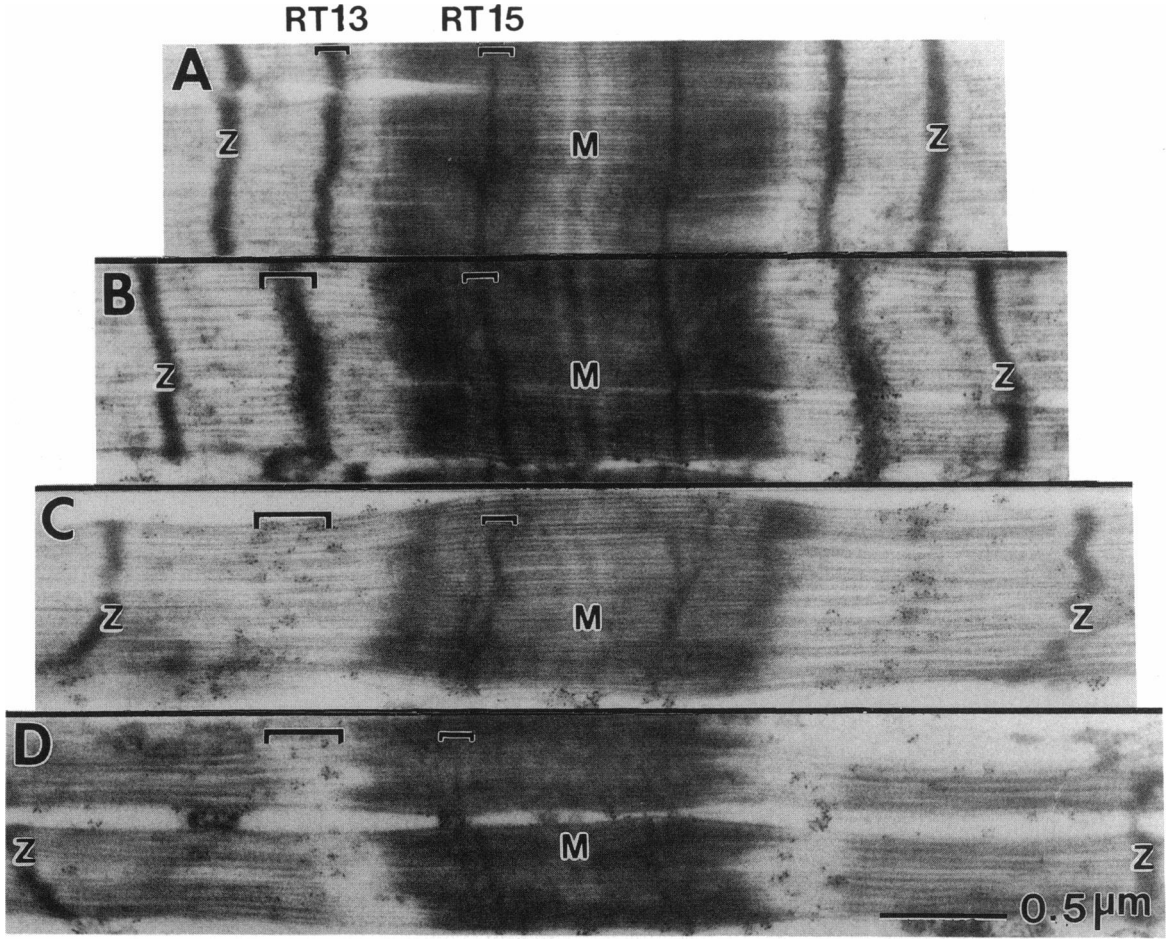

FIGURE 3 Segmental extensibility of titin filaments. Rabbit psoas split fibers were stretched to various lengths (up to 4.4 μm) in relaxing solution and double-labeled with mouse monoclonal antibodies, RT15 and RT13, which localize in the A- and I-bands, respectively. As the sarcomere length increased, the epitope of RT15 in the A-band remained stationary, whereas the epitope of RT13 in the I-band translocated away from the Z line. Additionally, the width of the epitope zone of RT13, as revealed by the gold particles, broadened slightly from *A* to *B* and significantly in *C* and *D*. Note the ragged appearances of the distal edges of the A-band in postyield sarcomeres (*C* and *D*), caused by excessive resting tension. Titin filaments spanned the gap regions of the nonoverlap sarcomere in *D*.

The translocation and zone spreading of RT13 epitope were analyzed by plotting antibody to Z line spacing (center to center) and epitope zone width as a function of sarcomere length of a large number of sarcomeres (>300). As shown in Fig. 4 *B*, a plot of Ab-Z versus *SL* is biphasic, consisting of two linear portions that intercept at a transition point (designated as SL_{RT13}) near 4 μm. RT13 translocated with a slope of 0.25 in sarcomeres below 4.0 μm. Above 3.8 μm, the epitope zone broadened significantly and rendered more scattering in the Ab-Z spacing data points. Statistical analysis of the centroid position of the epitope zones by moving average analysis revealed a slope of 0.11, representing a 40–50% reduction. Similar analysis indicated that the epitope zone broadened slightly (twofold from 2.2 to 4.0 μm) below a transition point of 4.0 μm (SL_{RT13}) and most drastically beyond 4.0 μm, with a 10-fold increase in slope and data scattering (Fig. 4 *C*).

To correlate titin extensibility with resting tension, the stretch curves of 17 split fibers were analyzed (Fig. 4 *A*). An average yield point of 3.8–3.9 μm was obtained. This value is strikingly similar to the transition point (SL_{RT13}) of both the epitope translocation curve and epitope zone spreading curve of the extensible segment of titin. Thus, the yield point of the sarcomere correlated with the transition point where titin filaments begin to undergo a change in extensibility. This correlation of mechanical and structural parameters provides strong and direct evidence that titin has a pivotal role in the development of resting tension. In particular, the stretching and linear extension of the extensible segment of titin filaments generate an exponential rise in resting tension.

Exponential phase and segmental extension of titin

The exponential phase of the resting tension–length curves has been analyzed by an equation first derived by Sten-Knudsen for whole muscle tissues (26) and subsequently modified by Magid (5) for detergent-skinned single fibers. The strain ϵ was defined as *fiber strain* (L/L_0) by Sten-Knudsen (26) and as *sarcomere strain* ($SL - SL_0/SL_0$) by Magid (5). Since our epitope translocation analysis indicated that the extension of a nonanchored titin segment is mainly responsible for resting tension development, we redefined ϵ as the *extensible segment strain* of the titin filament (E-segment) as:

$$\frac{F}{a} = \frac{E_0}{\alpha}(e^{\alpha\epsilon} - 1), \qquad (1)$$

where F is tension, a is the cross-sectional area of fiber, E_0 is initial modulus, α is a constant, and ϵ is extensible segment strain.

$$\epsilon = \frac{TL_E}{TL_{E0}} - 1, \qquad (2)$$

where TL is the contour length of titin and TL_{E0} and TL_E

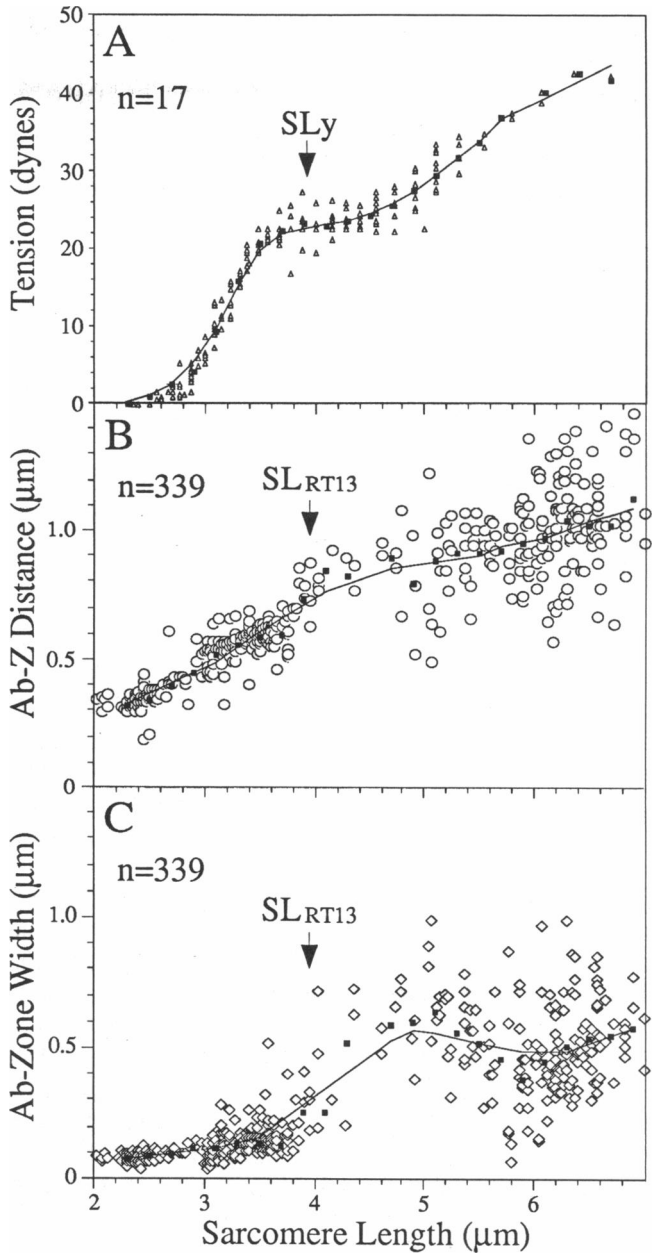

FIGURE 4 Correlation of yield point with transition points of titin epitope translocation curves. Tension, epitope spacing, and epitope zone width of a large number of rabbit psoas split fibers were recorded as a function of sarcomere length and analyzed statistically. For each panel, scatter plot, average values plot (■), and moving average plot are superimposed. (*A*) Passive tension–sarcomere length curves. Tension values of 17 fibers were normalized to the yield point, merged, classified, and analyzed. The multiphasic curve shows a yield point at 3.8 μm. (*B*) Epitope translocation curve of RT13. Epitope spacing, defined as the center to center distance between epitope and the Z line (Ab-Z) of 339 sarcomeres, was plotted as a function of sarcomere length. A transition point (SL_{RT13}) of the biphasic curve occurs at 3.8–4.0 μm. (*C*) Epitope zone spreading of RT13. Epitope zone width, measured from the spread of gold beads, of 339 sarcomeres was plotted as a function of sarcomere length. The zone width spreads significantly beyond 3.8–4.0 μm (SL_{RT13}).

are the contour length of the E-segment at slack sarcomere length (SL_0) and at a higher sarcomere length (SL), respectively. Since TL is approximately one half SL (i.e., each titin spans from the M line to the Z line) and TL_A (the length of the anchored segment of titin) may be estimated as half of the A band width, it follows that the extensible segment strain can be calculated from TL_E ($=TL - TL_A$) as the ratio of I-band width:

$$\epsilon = \frac{TL_E}{TL_{E0}} - 1 \approx \frac{SL - A}{SL_0 - A} \approx \frac{SL - SL_0}{SL_0 - A}, \qquad (3)$$

where $A = A_0$ in preyield sarcomeres (i.e., rest length A-band width). However, $A \leq A_0$ in postyield sarcomeres (see below).

The tension–length curves of a large number (>100) of fresh split fibers were collected and analyzed with this equation. For statistical analysis, all tension data were first normalized to the same cross-sectional area by expressing tensions as relative values to the yield point tension of the same fiber. In the example shown in Fig. 4 *A*, relative tension at a given sarcomere length were summed for 17 fibers with closely similar SL_y's (>90% of psoas fibers have SL_y's within 0.2 μm) and averaged to construct a generalized tension–length curve. This statistically averaged curve of the exponential phase was fitted by Eq. 1 to give $\alpha = 1.59$ and $aE_0 = 3.98$, with $SL_0 = 2.3$ μm and $A_0 = 1.6$ μm.

As the sarcomere was stretched near the yield point, the rise in tension began to deviate negatively from the exponential relationship. This was easily detected by the nonlinearity of a plot of log tension versus SL (cf. Fig. 6, *insets*). Only data points in the linear portion of these plots were subsetted for curve fitting as described above.

Our analysis indicated that the exponential phase of resting tension was modeled satisfactorily by a linear extension of the titin extensible segment. That the titin does indeed extend in a linear manner was demonstrated by the linear slope of Ab-Z versus SL plots of titin epitope translocations studies of rabbit psoas and several other muscle tissues (16, 27, 28). Thus, the elasticity of titin deviates from a simple Hookean spring.

The yield point and deformation of titin-thick filaments anchorage

Upon further stretching, tension eventually reached a maximum at the yield point and leveled off beyond 3.8 μm. Such a qualitative change is likely to reflect the onset of structural alteration of the sarcomere matrix, because intermediate filaments do not yet bear tension at this length. To reveal structural changes in postyield sarcomeres, we extended ultrastructural studies to highly stretched split fibers (Fig. 5). It was observed in electron micrographs of sarcomeres stretched beyond 3.8 μm, thin and thick filaments no longer overlap and structural distortion began to occur in the A-bands (Fig. 5 *B*). Frequently, subgroup or small bundles of thick filaments were pulled out of lateral alignment in both directions, producing A-bands with rough edges of lowered density and zig-zagged M lines (Fig. 5 *B*). Individual thick filaments gradually tapered into the slender titin filaments spanning the gaps between the edges of A-bands and IZI segments. It appeared as if the distal ends of thick filaments were distorted when subjected to yield point tension. Because it is difficult to trace the full length of individual thick filaments in plastic sections due to superposition of filament images, we estimated the average thick filament length by comparing A-band widths of pre- and postyield sarcomeres. For this purpose, the density profile of each A-band projected in the longitudinal direction was measured (see Experimental Procedures), and average A-band width was measured at half band height of the density profile. As shown in Fig. 5 *B*, average thick filament length decreased 10% from 1.6 μm in a preyield sarcomere to 1.45 μm in postyield sarcomeres at 3.9 μm. Overall, the reduction in A-band width ranges from 5 to 18% for rabbit psoas muscle at 3.9–4.2 μm.

A likely consequence of the distortion near the ends of thick filaments is the dislodging of titin–myosin filament anchorage near the border of the A-band. Supporting this idea are the observations that the elastic translocation of titin epitope RT13 is altered in postyield sarcomeres and that there are considerable broadening of epitope zones after the yield point (Fig. 4). Indeed, a decrease in slope of the Ab-Z versus SL plot of postyield sarcomeres would be expected if an additional length of titin is recruited from the anchored segment in the A-band. The appreciable zone broadening is also consistent with a net but appreciable increase in the length of the extensible segment in postyield sarcomeres. Taken together, our data suggest that a portion of the previously constrained titin segment is released from the distal region of thick filaments that were distorted by the stress at yield point. It was noted, however, that the edges of truncated A-bands were fuzzy and jagged, suggesting that thick filaments are probably no longer uniform in length and that the released titin segments may have a broad length distribution. This heterogeneity may have contributed to the considerable scattering of data points beyond the yield point in both epitope translocation and epitope spreading curves (Fig. 4).

Thus, to account for both the structural change in thick filaments and the change in translocation behaviors of titin, we propose that the yield point represents the onset of a partial conversion of the anchored A-segment to extensible segment of titin as a result of the distortion of the distal ends of thick filaments (see Discussion).

Reduced stiffness of postyield sarcomeres

Because a net length increase in the extensible titin segment of postyield sarcomeres is expected to affect the stiffness of the sarcomere, we tested this prediction by

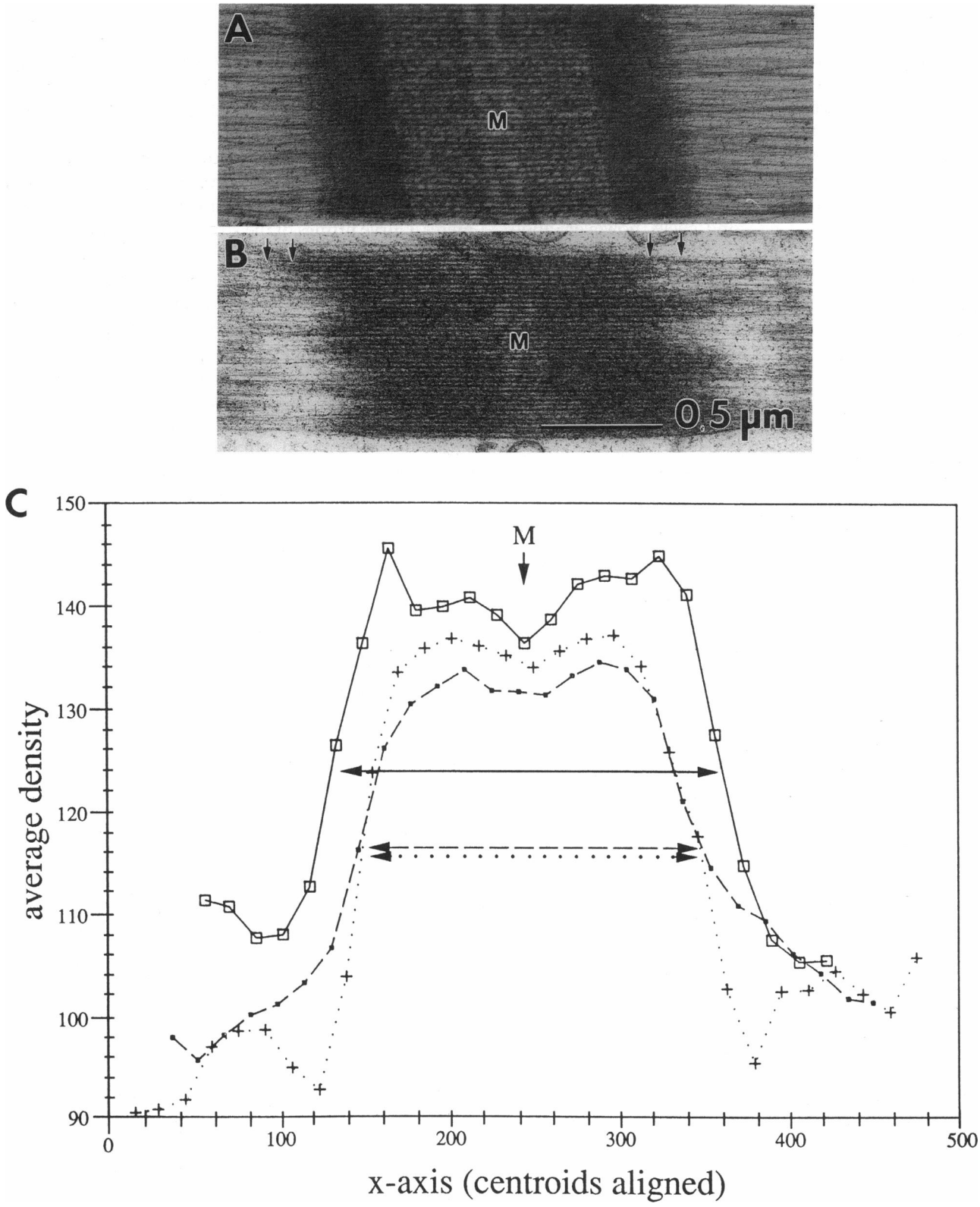

FIGURE 5 Average thick filament length in highly stretch sarcomeres. The average length of thick filaments in postyield sarcomeres was estimated by determining the A-band width from density profiles of digitized electron micrographs such as those in *A* and *B*. Gray-level profiles for three different A-bands are shown in *C*: one from a preyield sarcomere (□) and two from postyield samples (+ and ●). A-band widths, as measured at the half band height from the profiles (arrow-headed lines in *C*), showed a 12–18% reduction in overly stretched sarcomeres. Note the fuzzy edges of the A-band and misalignment of thick filaments in the overly stretched sarcomere (*arrows* in *B*) in contrast to the sharper edges in *A*.

subjecting the same split fiber to several cycles of stretch–release. In one set of experiments, a split fiber was subjected first to one preyield cycle (Fig. 6 *A*), followed by three postyield cycles with increasingly higher degrees of stretch from 3.4 to 4.6, 5.0, and 5.6 μm, respectively (Fig. 6, *B–D*). The preyield stretch (Fig. 6 *A*) caused no change in stiffness in cycle 2, with superimposable stretch curve and an identical slope of the linear portion of log tension versus *SL* plot (Fig. 6 *B*). The postyield stretches in the second cycle, however, abolished the yield point at 3.8 μm in subsequent cycles (Fig. 6, *C* and *D*). Furthermore, stiffness in cycles 3 and 4 dropped significantly, as indicated by the smaller slopes of the log tension versus *SL* plots (Fig. 6, *C* and *D, insets*). It is interesting that the preyield stretch caused no increase in slack sarcomere length SL_0 in cycle 2, but postyield stretches (cycles 2 and 3) caused the slack sarcomere length to increase from 2.3 μm in cycle 2 to 2.4 μm in cycle 3 and 2.5 μm in cycle 4.

It is important to note that although the tension in the stretch curves of cycle 3 and 4 were significantly depressed between 2.3 and 4.1 μm as compared with that of cycle 1 and cycle 2, it eventually rose above the yield point tension value at higher sarcomere lengths. These observations suggest that the high stress at or beyond the yield point caused an irreversible structural alteration that led to a reduction in stiffness, an increase in slack sarcomere length, but a retension of full force-bearing capacity.

In a second set of experiments, a split fiber was subjected to four cycles of postyield stretch–releases up to 4.6 μm (Fig. 6, *E–G*) or 5.6 μm (Fig. 6 *H*). As expected, the first postyield stretch (cycle 1, Fig. 6 *E*) abolished the yield point at 3.8 μm, caused the reduction in stiffness, and an increase in slack length in subsequent cycles (from 2.3 μm in cycle 1 to 2.5 μm in cycles 3 to 4). It is interesting that postyield cycles 2, 3, and 4 are nearly superimposable, having been subjected to the same degree of stretch. Again, the force bearing capacity was not affected by postyield stretches, as the tension above 4.1 μm invariably rose to the same level as that of cycle 1.

These two sets of experiments exemplify the common behavior of a large number of split fibers that we studied ($n > 100$), all of which suggest that the high stress at and beyond the yield point caused irreversible structural alterations that vary in magnitude with the degree of sarcomere stretch. However, the force-bearing capacity of titin filaments remain essentially intact and the observed reduction in tension and stiffness at moderate stretch (e.g., below 4.1 μm) cannot be attributed solely to severing or complete detachment of titin filaments, since such changes would lead to a proportional reduction at *all* degrees of sarcomere stretch. Instead, the observed stiffness and slack length changes are most likely due to architectural rearrangements that resulted in a net length increase of the extensible segment of titin filaments.

To evaluate this concept quantitatively, we analyzed the stretch curves of the various cycles of postyield sarcomeres by Eq. 1. For this purpose, the segment strain, ϵ_n, for the nth cycle is generalized as $SL_n - SL_{on}/SL_{on} - \tilde{A}_n$, where SL_n, SL_{on}, and $\tilde{A}_n$ are the sarcomere length, slack sarcomere length, and average length of anchored titin segment, respectively. This redefinition incorporates the observations that slack sarcomere length and anchored titin segment length may be different in postyield sarcomeres. Curve fittings of the stretch curves in Fig. 6, *A* and *D* indicated that the exponential phase of cycle 1 (preyield sarcomeres) are $SL_0 = 2.3$ μm, $A_1 = 1.6$ μm, and $\alpha = 1.8$ and $aE_0 = 1.9$. The exponential phase of cycle 4 (postyield sarcomere) fitted well with $SL_{04} = 2.5$ μm, $A_4 = 1.45$ μm, $\alpha = 1.8$, $aE_0 = 1.9$. Alternatively, plots of tension versus segment strain E_n for the four stretch curves are nearly superimposible (not shown). These observations indicate that the newly recruited titin segments in postyield sarcomeres behave in a similar fashion as the I-segment in preyield sarcomeres. Essentially the same conclusion was reached for stretch curves in Fig. 6, *E* and *H* (not shown).

Such a comparison clearly indicates that the functional form of Eq. 1 applies to all cycles and that the reduction in stiffness of the exponential phase in cycles subsequent to a postyield stretch could be explained satisfactorily by a net increase in slack contour length of the extensible segment that accompanied a reduction in thick filament length. In other words, the data can be explained without invoking a change in the number and intrinsic extensibility of titin filaments in postyield sarcomeres. Significantly, the calculated average anchored segment length, A_n, from curve fitting of mechanical measurements agreed with the average thick filament length determined by electron microscopy and the density profile averaging technique (cf. Fig. 5). Taken together, our data strongly support the idea that yield point marks the onset of structural distortions, including thick filament truncation and the dislodging of titin–myosin anchorages near the distal ends of the thick filaments. According to this analysis, postyield sarcomeres are more compliant for a simple reason: at a given *sarcomere strain,* the longer extensible segments yielded a lower *segment strain.*

Extensibility of released A-segment of titin filaments

The mechanical behaviors of postyield sarcomeres suggest that a portion of the A-segment titin, once relieved of the structural constraints imposed by adhering thick filaments, become extensible. The degree of extension of the released titin in postyield sarcomeres can be estimated as $\frac{1}{2}(SL - SL_y)/\frac{1}{2}(A_0 - A_n)$, where $\frac{1}{2}(SL - SL_y)$ represents the extended length of the released segment and $\frac{1}{2}(A_0 - A_n)$ equals the unstrained contour

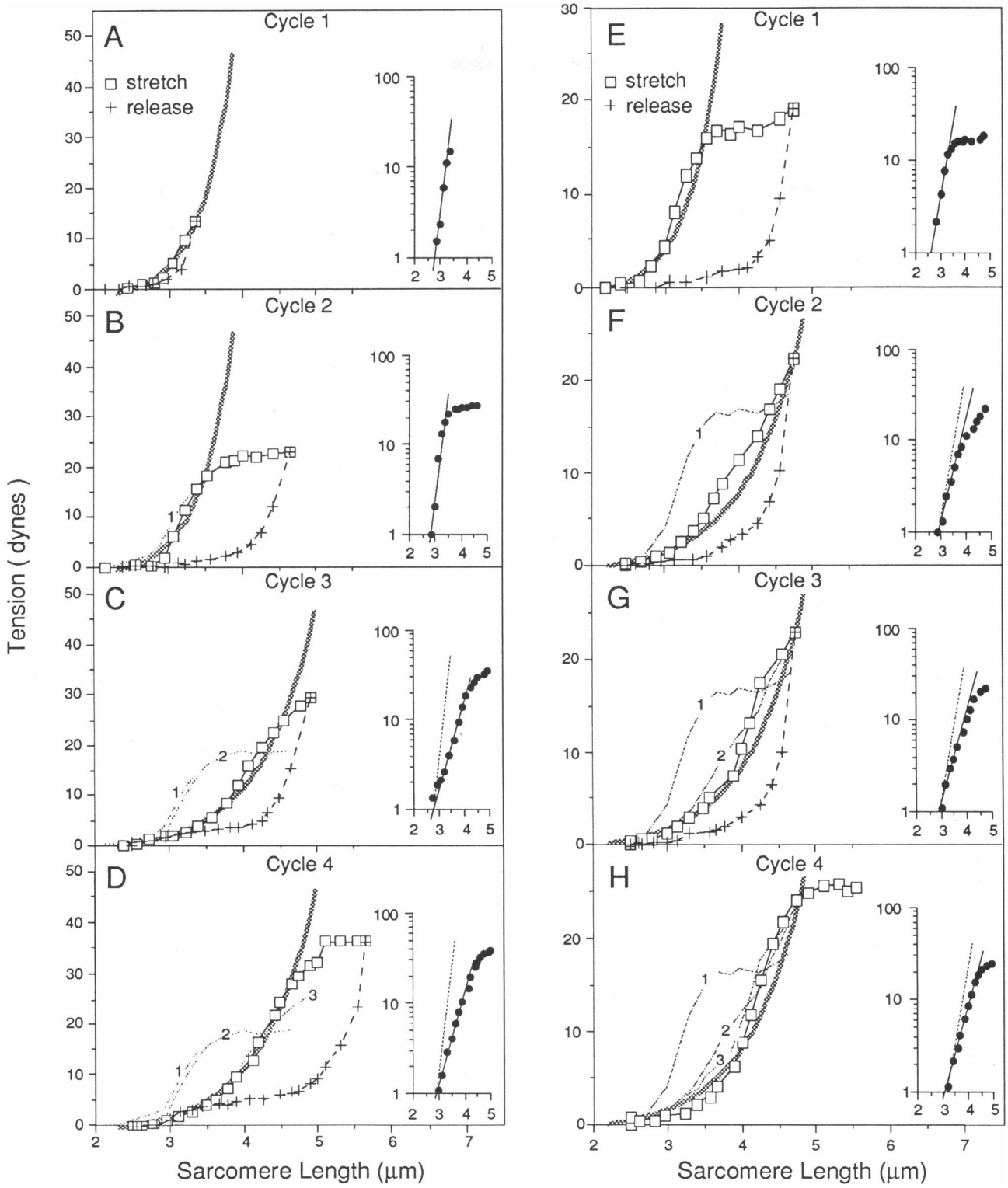

FIGURE 6 Tension–length loops of passive fibers subjected to successive preyield and postyield cycles of stretch–releases. To facilitate comparisons, stretch curves of previous cycles were superimposed as light dotted lines labeled with 1, 2, or 3. The thick exponential curves (extending beyond data points) represent the exponential fit according to Eq. 1 (see text). (*A–D*) A single split fiber was subjected to a preyield stretch–release cycle (*A*) followed by three postyield cycles (*B–D*). (*E–H*) A single split fiber was subjected to four cycles of postyield stretch–releases. (*A* to *H, insets*) Plots of log (tension) versus sarcomere length for the stretch curves of each cycle. The straight line for each cycle represents data points selected for exponential curve fitting by Eq. 1. To facilitate comparison, the straight line for cycle 1 (*dotted line*) is superimposed on subsequent plots.

length of the released segment. At 4.6 μm (Fig. 6, *F* and *G*), this extension ratio of released A-segment is approximately four and is strikingly similar to that of the extensible segment of preyield sarcomeres at the yield point. Thus, the released A-segment, which is structurally and mechanically in series with the E-segment, extends to a similar degree under identical stress.

It was noted that preyield cycles did not alter sarcomere slack length between cycles. In contrast, postyield stretches (to 6 μm) frequently caused upon total release an increase in slack length (Fig. 6) that corresponded approximately to the reduction of A-band width (Fig. 5). This increase in slack length suggests that titin may be compressed when complexed with myosin filaments in the A-band and stress-induced release caused the released titin segment to assume a longer span at slack sarcomere length. Alternatively, released A-segment may still be associated with fragmented thick filaments that prevent titin from returning to its slack length upon release, but such extraneous material exerts no effect on its extensibility upon stretch (see Fig. 8).

Although the release of a short length of titin A-segment satisfactorily explains the reduction in stiffness and the abolishment or shift of yield point in subsequent stretches, additional factors must be invoked to explain why resting tension due to sarcomere matrix leveled beyond yield point and did not continue to rise upon further stretch (Fig. 2). The leveling of tension may be explained if further stretch pulls and converts additional A-segment titin. As a result of this continuous lengthening of extensible segment, the tension would stay constant at the yield point value. Experimental testing was difficult, however, since sarcomeres tended to be torn apart beyond 6 μm.

Yield point tension per titin filament

To measure the force-bearing capacity of titin filaments, two split fibers were subjected first to one cycle of postyield stretch–release and then fixed and processed for electron microscopy. Thick filament counting across the fiber cross-sectional area gave an average of 1.11×10^6 thick filaments (1,321 thick filaments per μm^2 of myofibrillar cross-sectional area), the yield tension was calculated to be 1.53×10^{-5} dynes per thick filament (7, 29). Because there are an average of six titin polypeptides per half-thick filament (7, 11, 12), the average force-bearing capacity for the extensible segment is 2.5×10^{-6} dyne/titin polypeptide at the yield point.

Epitope translocation of A-band extracted sarcomeres

The intrinsic extensibility of the A-segment of titin was also demonstrated by epitope translocation studies of an titin epitope in the A-segment of titin filaments. As shown in Fig. 7, the pair of doublet epitopes recognized by monoclonal RT15 remain stationary in the A-band (at 0.4 μm from the M line) in sarcomeres stretched up to 5 μm. In sarcomeres that have been treated with a 0.6 M KCl buffer to extract thick filaments, most titin filaments were dislodged from their anchorage at the M line. However, some residual titin filaments remained attached at the M line and maintained their longitudinal continuity to the Z line (Fig. 7 *B, inset*). In these sarcomeres, the RT15 epitopes, discernable by the gold beads labeling, were found to move away from the M line. Plots of Ab to M distance as a function of sarcomere length clearly revealed that the RT15 epitope translocated elastically, when freed of thick filament constraints (Fig. 7 *B*). These behaviors are consistent with the idea that titin filament is intrinsically extensible along its entire length, and its interaction with thick filaments rendered a large segment of titin inextensible.

DISCUSSION

Sarcomere matrix and intermediate filament network as interlinked force-bearing lattices

Our studies demonstrated that both the endosarcomeric matrix and exosarcomeric intermediate filament network are force-bearing lattices within the skeletal muscle cell. The successful "dissection" of the tension–length curves of sarcolemma-free muscle fibers into two independent (i.e., additive) components, each arising from a distinct lattice was made possible by our previous observation that the KI treatment not only dissolved thick and thin filaments (25, see also 28) but also dislodged titin filaments from their M line anchorage (10). As a result, only the KI-resistant intermediate filaments retained their structural connectivity and force-bearing capacity in the KI residue. Quantitative analysis of mechanical responses was also facilitated by the use of a cycling regime to compare changing behaviors of the *same* split fiber that has been subjected to extraction or various degrees of stretch. For statistical analysis of fiber populations and comparison among different fibers, normalization of tensions relative to the individual yield point value before averaging was effective (Fig. 4). Our current working hypothesis is depicted graphically in Fig. 8 and further elaborated below.

Viscoelasticity of intermediate filament network

Although a mechanical role of intermediate filaments in striated muscles has been speculated widely (6, 8–10), very few direct measurements have been performed on either filaments reconstituted from purified proteins or on the filamentous network that surrounds sarcomeres (25). Our measurements indicate that the exosarcomeric lattice can bear significant tension but only at very

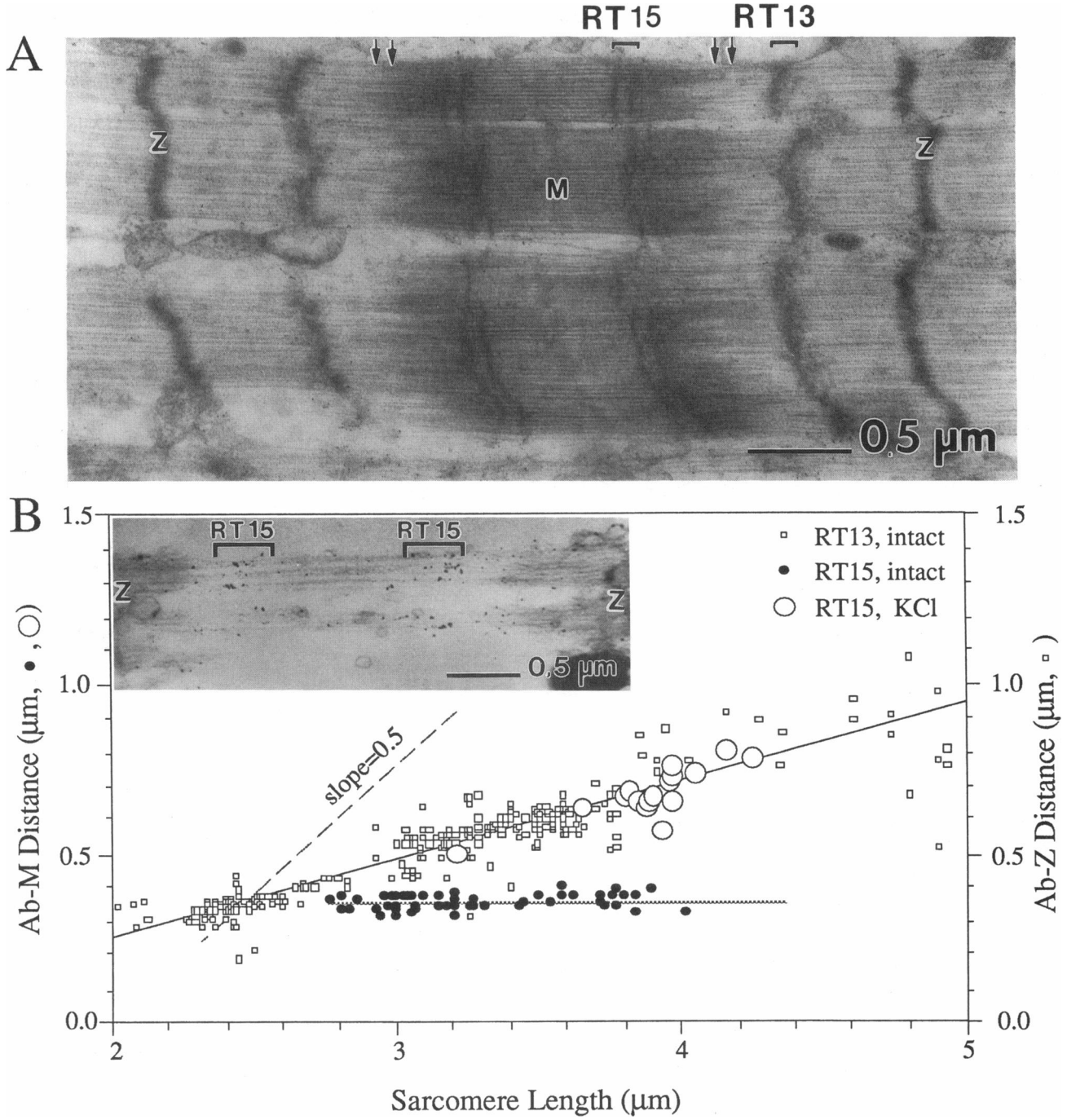

FIGURE 7 Intrinsic extensibility of the A-segment of titin filaments. (*A*) A rabbit psoas split fiber stretched to postyield length was dual-labeled with RT13 to label a single I-band epitope and with RT15 to stain a doublet in the A-band per half sarcomere. The epitope bands remain sharp despite the ragged appearance of edges of A-band (*arrows*). (*B, inset*) A split fiber was extracted with a 0.6 M KCl buffer to remove the A-band before immunolabeling with RT15. Gold beads were found mainly on the residual titin filaments that span the IZI segments of the sarcomere. (*B*) Plots of Ab to Z distance (RT13, intact), Ab to M distance (RT15, intact), and Ab to mid-sarcomere distance in 0.6 M KCl extracted samples (RT15, KCl) as a function of sarcomere length. Note that RT15 remained stationary in intact sarcomeres, but translocated elastically in A-band extracted sarcomeres, with a slope of Ab-M versus *SL* plot that is coincidently the same as that of Ab-Z versus *SL* for RT13 in the I-band.

high extension of muscle (>4.5 μm). For rabbit psoas split fibers, the intermediate filament network is viscoelastic and displays small but reproducible hysteresis in stretch–release cycles. It contributed as much as 20–50% of the total fiber tension before fibers broke near 5.5–6.5 μm (Fig. 3).

Our data thus indicate that the intermediate filament network that connects Z lines and M lines of adjacent

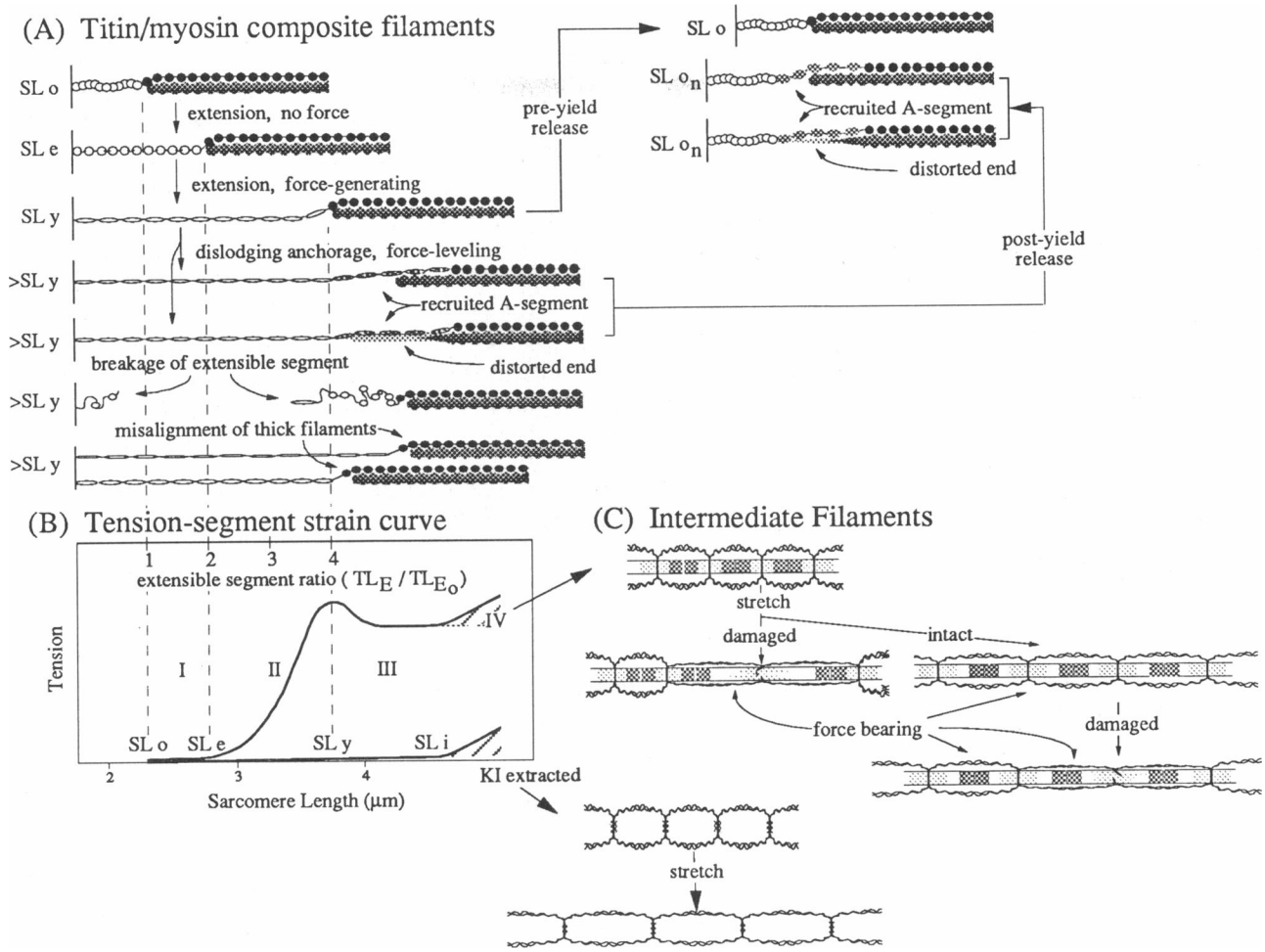

FIGURE 8 Proposed structural correlates of tension–segment strain curves of sarcomere-associated cytoskeletal lattices. The resting tension–sarcomere length curve (*B*) is characterized by four zones (I to IV) and interpreted by structural behaviors of the sarcomere matrix (*A*) and the intermediate filament lattice (*C*). *Zone I.* From SL_0 to SL_e. The stretching of the sarcomere in this range generates no significant tension, perhaps reflecting a straightening of a flaccid network of titin filaments without a change in contour length. *Zone II.* From SL_e to SL_y. The stretching of sarcomere generates exponential rise in tension and causes a net change in the contour length of the extensible segment of titin filaments. Release of the preyield fibers returns the sarcomeres to prestretch slack length (SL_0). *Zone III.* Yield point and beyond ($> SL_y$). The yield point tension causes distortion of distal ends of thick filaments and the dislodging of titin–myosin anchorage. The recruitment from the anchored segment causes a net increase in the length of the extensible segment and a reduction of stiffness. Misalignment and breakage of titin may also contribute to the broad transition near the yield point. Release of postyield fibers at the $(n-1)$th cycle returns it to a new slack sarcomere length SL_{on} that is longer than the SL_0 of preyield sarcomeres. The increase in slack length reflects the net length of the newly recruited titin filaments. The net length of the extensible segment increases further when sarcomeres are stretched beyond the yield point, resulting in a leveling of tension. *Zone IV.* Intermediate filaments. The intermediate filament lattice that links adjacent sarcomeres at the Z-line (shown) and M-line (not shown) is normally slack and begins to elongate and bears tension around 4.5 μm. Below 4.5 μm, the intermediate filaments may also elongate locally if sarcomeres lose the ability to generate and transmit active force. In such cases, intermediate filaments may serve as a bypass mechanism to transmit tension to prevent a total breakdown of force transmission between adjacent sarcomeres in the myofibril. The generalized tension–segment–strain curve is plotted against the extensible segment ratio (TL_E/TL_{E_o}), which is approximated by the ratio of I-band width at various sarcomere lengths. The resting tension–sarcomere length curves of many types of muscles can be normalized to this tension–segment–strain curve.

sarcomeres longitudinally and transversely in the myofibril may be unstrained within the physiological range of muscle extension and contributes little to the transmission of resting tension. As depicted graphically in Fig. 8 *C*, it is conceivable, however, that in cases where sarcomeres are damaged and incapable of transmitting either active or resting tension, the associated intermediate filaments may be stretched to a force-bearing length by adjacent functioning sarcomeres and thus provide mechanical continuity. Its potential role as a mechanical bypass device has been proposed previously (10). The filaments of the network that connect parallel myofibrils transversely has been implicated in transmitting tension in the radial direction of the muscle fibers (9). It is worth noting that since sarcolemma and the membrane-associated intermediate filaments (costamere) were re-

moved in our split fiber preparations, their mechanical properties were not addressed.

Viscoelasticity and yield point of the sarcomere matrix

The stretch–response of the sarcomere matrix, as deduced by subtracting the contribution of intermediate filaments (i.e., KI residue curve) from the multiphasic curve of the split fiber, displays a characteristic biphasic tension–length curve: the tension rises exponentially and levels off at and beyond the yield point (Fig. 3). This yielding indicates that the sarcomere matrix has reached an elastic limit since it can extend easily without additional stress. Once over its elastic limit, the sarcomere matrix is rendered irreversibly more compliant in subsequent stretches (Fig. 6).

Such stretch responses of the sarcomere matrix can be understood qualitatively and quantitatively on the basis of the reversible extension of a segment of titin that is anchored between the Z line and the end of thick filaments: in preyield point sarcomeres, linear extension of this segment gives rise to an exponential rise of resting tension that has been described previously by many investigators (1, 25–27, 29). Beyond the yield point, the unstrained length of the extensible segment becomes longer by incorporating a section of the previously anchored titin segment that is released near the ends of thick filaments (Figs. 3 *A* and 8). The distal ends of the thick filaments in postyield sarcomeres may have been deformed or fragmented by the yield point tension that is exerted at these loci by titin (Fig. 5). Alternatively, titin–myosin anchorage near the distal ends may be shifted toward an internal site without concomitant structural damages to the thick filaments (Fig. 8 *A*). Whatever the mechanism, the release of titin appears to be localized and in small scale. Structural analysis indicated ≤ 0.15 μm recruitment per half sarcomere up to 5.5 μm. It is interesting that this value coincides with the increase in slack sarcomere length. Our data thus suggest that the released titin spans about twice the original value in the anchored state.

According to our analysis, the exponential phases of tension–length curves of both pre- and postyield sarcomeres satisfy the same quantitative relationship if the extension ratio of the entire extensible segment and associated structural changes are taken into consideration in Eq. 1. Postyield sarcomeres become more compliant for a simple reason: for a given amount of *sarcomere strain* ($SL - SL_0$), the longer extensible segment leads to a smaller titin *segment strain* and thus a lower *sarcomere stress*. There was thus no need to invoke additional factors such as major changes in the intrinsic elastic property of the original extensible segments or a completely different intrinsic elasticity of A-segment, because both the recruited A-segment and the original extensible segment have the same E_0 and α (Fig. 6). The possibility of subtle changes, however, cannot yet be ruled out.

It is also conceivable that misalignment of thick filaments within the A-band, observed as staggered M lines in highly stretched sarcomeres (Figs. 3 and 5), may be involved in the yielding of the sarcomere and indeed may have contributed to the broadening of the tension–length curve near the yield point (Fig. 8). Such a factor can only be of secondary importance, however, because only short range sliding (~ 0.2 μm) of thick filaments occurred under our conditions of slow stretching, which is unlikely to result in a leveling of tension lasting ≤ 1.5 μm beyond the yield point (Figs. 2 and 6).

Tension–length curves and segmental strain of titin

With yield point as a landmark, the resting tension–sarcomere length can be divided into four zones, each with a distinct structural interpretation.

Zone I. From resting length (SL_0) to the onset of exponential increase in tension (SL_e). No significant tension is generated below the segment extension ratio of 1.7. This could result from a straightening of flaccid titin filaments without a net change in contour length.

Zone II. From onset of exponential tension (SL_e) to yield point. Tension increases exponentially and subsequently deviates from exponential and reaches a broad local maximum near an extension ratio of 4.0. In this zone, titin extends its contour length linearly, perhaps by unfolding protein chains in a force-bearing mode.

Zone III. Yield point and beyond ($> SL_y$). The tension reaches a maximum and then declines slightly. This reduction may be caused by a net increase in the length of the extensible titin segment newly recruited from the A-band region. Further stretch beyond the yield point may cause increasingly more titin to be converted to the extensible segment, thus restricting the maximum tension on the titin filament to that of the yield point level.

Zone IV. From 4.5 μm and beyond. The second tension rise reflects the additional contribution of the intermediate filament network that surrounds each myofibril.

In this article we have shown that this segmental strain concept is applicable to the understanding of the yield phenomena in highly stretched skeletal muscle fibers. Elsewhere we have shown that this concept is equally powerful in explaining features of the resting tension–sarcomere length curves of six rabbit skeletal muscles that express three size classes of titin isoform (27, see also 29): the muscle with the longer titin displays a longer extensible segment and therefore longer SL_e and SL_y. It is striking that the yield point for each of the six muscles occurs at an extension ratio of 4.0. Our recent studies of the resting tension curves of waterbug indirect flight muscle, which has a long A-band (2.65 μm) and short

I-band (0.05 μm), revealed that the yield point occurred at very short (6%) sarcomere strain (30). Interestingly, the yield point is reached at a segment strain of minititin at 3.2, similar to that of vertebrate skeletal muscles. Additionally, postyield extension caused a pronounced increase in the slack sarcomere length and caused a stiffness reduction that can be understood quantitatively based on the segment strain of minititin (30). We further noted that the yield point of rat cardiac muscle also appears to occur at an extension ratio of ~3.5 (27). It is curious why the yield points of so many muscles occur near this extension ratio. We suspect that this ratio may reflect a general design principle of the titin–myosin composite filament: the adhesive strength between titin and myosin is designed to maximally withstand the characteristic tension that is generated by individual titin isoform when extensible segment is extended three- to fourfold.

The various examples discussed above illustrate that the segment strain of the elastic filaments that link between the Z line and the ends of the thick filaments is important in understanding the resting tension–sarcomere length curves, including the shape, its tissue-specific isoform expression, as well as the yielding phenomena that underlies the reduction of the elastic modulus of highly strained sarcomeres. Thus, we propose that the interplay among four major factors determines the size and shape of the resting tension–sarcomere length curves: (*a*) the intrinsic molecular elasticity of titin, (*b*) the net contour length and the segment strain of the extensible segment, (*c*) the interaction strength of the titin–myosin composite filaments, and (*d*) the contribution of intermediate filaments at high sarcomere strain.

Mechanically, myosin and titin in the sarcomere act together and behave as a "filament-matrix" composite material at the molecular level. Below the elastic limit of the sarcomere, the deformation occurs exclusively in the pliant titin matrix. At larger strain, intrinsic properties of the stiff myosin filament and its interaction with titin begin to manifest themselves to prevent the rupturing of titin and the fracturing of the sarcomere. In essence, the myosin–titin composite filament acts as a dual-stage molecular spring with a built in high-strain limit.

We gratefully acknowledge stimulating discussions with Drs. A. Brady and H. Granzier. We also appreciate the thoughtful comments of the reviewers of this article. This work was supported by grants from Foundation for Research (to K. Wang and R. M. Carter) and NIH (20270 to K. Wang).

Received for publication 31 August 1992 and in final form 13 November 1992.

REFERENCES

1. Cooke, R. 1986. The mechanism of muscle contraction. *Crit. Rev. Biochem.* 21:53–118.
2. Huxley, A. F. 1974. Review lecture: muscular contraction. *J. Physiol.* 243:1–43.
3. Huxley, H. E., and M. Kress. 1985. Crossbridge behaviour during muscle contraction. *J. Muscle Res. Cell Motil.* 6:153–161.
4. Jewell, B. R., and D. R. Wilkie. 1960. The mechanical properties of relaxing muscle. *J. Physiol. (Lond.).* 152:30–47.
5. Magid, A. 1985. Myofibrils bear most of the resting tension in frog skeletal muscle. *Science (Wash. DC).* 230:1280–1282.
6. Price, M. G. 1991. Striated muscle endosarcomeric and exosarcomeric lattices. *Adv. Struct. Biol.* 1:175–207.
7. Wang, K. 1985. Sarcomere-associated cytoskeletal lattices in striated muscle. *In* Cell and Muscle Motility. J. W. Shay, editor. Plenum Publishing Corporation, New York. 315–369.
8. Lazarides, E. 1980. Intermediate filaments as mechanical integrators of cellular space. *Nature (Lond.).* 283:249–256.
9. Street, S. F. 1983. Lateral transmission of tension in frog myofibers: A myofibrillar network and transverse cytoskeletal connections are possible transmitters. *J. Cell. Physiol.* 114:346–364.
10. Wang, K., and R. Ramirez-Mitchell. 1983. A network of transverse and longitudinal intermediate filaments is associated with sarcomeres of adult vertebrate skeletal muscle. *J. Cell Biol.* 96:562–570.
11. Maruyama, K. 1986. Connectin, an elastic filamentous protein of striated muscle. *Int. Rev. Cytol.* 104:81–114.
12. Trinick, J. 1991. Elastic filaments and giant proteins in muscle. *Curr. Opin. Cell Biol.* 3:112–118.
13. Wang, K. 1992. Nebulin. *In* Cytoskeletal, Extracellular Matrix and Adhesion Proteins. T. Kreis, and R. Vale, editors. Oxford University Press, Oxford. In press.
14. Wang, K. 1992. Titin. *In* Cytoskeletal, Extracellular Matrix and Adhesion Proteins. T. Kreis and R. Vale, editors. Oxford University Press, Oxford. In press.
15. Furst, D., M. Osborn, R. Nave, and K. Weber. 1988. The organization of titin filaments in the half sarcomere revealed by monoclonal antibodies in immunoelectron microscopy: A map of ten nonrepetitive epitopes starting at the Z line extends close to the M line. *J. Cell Biol.* 106:1563–1572.
16. Itoh, Y., J. Suzuki, S. Kimura, K. Ohashi, H. Higuchi, H. Sarvada, and T. Shimizu. 1988. Extensible and less-extensible domains of connectin filaments in stretched vertebrate skeletal muscle sarcomeres as detected by immunofluorescence and immunoelectron microscopy using monoclonal antibodies. *J. Biochem.* 104:504–508.
17. Labeit, S., M. Gautel, A. Lakey, and J. Trinick. 1992. Towards a molecular understanding of titin. *EMBO (Eur. Mol. Biol. Organ.) J.* 11:1711–1716.
18. Wang, K., and R. Ramirez-Mitchell. 1983. Ultrastructural morphology and epitope distribution of titin—a giant sarcomere-associated cytoskeletal protein. *J. Cell Biol.* 97:968*a*. (Abstr.)
19. Whiting, A., J. Wardale, and J. Trinick. 1989. Does titin regulate the length of muscle thick filaments? *J. Mol. Biol.* 205:263–268.
20. Horowits, R., E. S. Kempner, M. E. Bisher, and R. J. Podolsky. 1986. A physiological role for titin and nebulin in skeletal muscle. *Nature (Lond.).* 323:160–164.
21. Higuchi, H. 1992. Changes in contractile properties with selective degestion of connectin (titin) in skinned fibers of frog skeletal muscle. *J. Biochem.* 111:291–295.
22. Horowits, R., K. Maruyama, and R. J. Podolsky. 1989. Elastic behavior of connectin filaments during thick filament movement in activated skeletal muscle. *J. Cell Biol.* 109:2169–2176.
23. Horowits, R., and R. J. Podolsky. 1988. Thick filament movement and isometric tension in activated skeletal muscle. *Biophys. J.* 54:165–171.

24. Wang, K., and J. Wright. 1988. Architecture of the sarcomere matrix of skeletal muscle: immunoelectron microscopic evidence that suggests a set of parallel inextensible nebulin filaments anchored at the Z line. *J. Cell Biol.* 107:2199–2212.

25. Higuchi, H., and Y. Umazume. 1985. Localization of the parallel elastic components in frog skinned muscle fibers studied by the dissociation of the A- and I-bands. *Biophys. J.* 48:137–147.

26. Sten-Knudsen, O. 1953. Torsional elasticity of the isolated cross striated muscle fibre. *Acta Physiol. Scand.* 28:1–240.

27. Wang, K., R. McCarter, J. Wright, J. Beverly, and R. Ramirez-Mitchell. 1991. Regulation of skeletal muscle stiffness and elasticity by titin isoforms: A test of the segmental extension model of resting tension. *Proc. Natl. Acad. Sci. USA.* 88:7101–7105.

28. Roos, K. P., and A. J. Brady. 1989. Stiffness and shortening changes in myofilament-extracted rat cardiac myocytes. *Am. J. Physiol.* 256:H539–H551.

29. Horowits, R. 1992. Passive force generation and titin isoforms in mammalian skeletal muscle. *Biophys. J.* 61:392–398.

30. Granzier, H. L. M., and K. Wang. 1992. Interplay between passive tension and strong and weak cross-bridges in insect asynchronous flight muscle: A functional dissection by gelsolin mediated thin filament removal. *J. Gen. Physiol.* 101:235–270.